Biomedical Optics EXPRESS

Contact-free monitoring of circulation and perfusion dynamics based on the analysis of thermal imagery

Carina Barbosa Pereira,[1,*] Michael Czaplik,[2] Nikolai Blanik,[1] Rolf Rossaint,[2] Vladimir Blazek,[1] and Steffen Leonhardt[1]

[1]*Chair for Medical Information Technology, Helmholtz Institute for Biomedical Engineering, RWTH Aachen University, Pauwelsstrs. 20, D-52074 Aachen, Germany*
[2]*Department of Anesthesiology, University Hospital RWTH Aachen, Pauwelsstrs. 30, D-52074 Aachen, Germany*
[*]*pereira@hia.rwth-aachen.de*

Abstract: Acute circulatory disorders are commonly associated with systemic inflammatory response (SIRS) and sepsis. During sepsis, microcirculatory perfusion is compromised leading to tissue hypoperfusion and potentially to multiple organ dysfunction. In the present study, acute lung injury (ALI), one of the major causes leading to SIRS and sepsis, was experimentally induced in six female pigs. To investigate the progress of body temperature distribution, measurements with a long-wave infrared camera were carried out. Temperature centralization was evidenced during ALI owing to impairments of peripheral perfusion. In addition, statistical analysis demonstrated strong correlations between (a) standard deviation of the skin temperature distribution (SD) and shock index (SI) ($p<0.0005$), (b) SD and mean arterial pressure (MAP) ($p<0.0005$), (c) $\Delta T/\Delta x$ and SI ($p<0.0005$), as well as between (d) $\Delta T/\Delta x$ and MAP ($p<0.0005$). For clarification purposes, $\Delta T/\Delta x$ is a parameter implemented to quantify the spatial temperature gradient. This pioneering study created promising results. It demonstrated the capacity of infrared thermography as well as of the indexes, SD and $\Delta T/\Delta x$, to detect impairments in both circulation and tissue perfusion.

OCIS codes: (040.3060) Infrared; (170.1610) Clinical applications; (170.2655) Functional monitoring and imaging.

References and links

1. R. P. Dellinger, M. M. Levy, J. M. Carlet, J. Bion, M. M. Parker, R. Jaeschke, K. Reinhart, D. C. Angus, C. Brun-Buisson, R. Beale, T. Calandra, J. F. Dhainaut, H. Gerlach, M. Harvey, J. J. Marini, J. Marshall, M. Ranieri, G. Ramsay, J. Sevransky, B. T. Thompson, S. Townsend, J. S. Vender, J. L. Zimmerman, and J. L. Vincent, "Surviving sepsis campaign: International guidelines for management of severe sepsis and septic shock: 2008," Intensive Care Med. **34**(1), 17–60 (2008).
2. M. M. Levy, M. P. Fink, J. C. Marshall, E. Abraham, D. Angus, D. Cook, J. Cohen, S. M. Opal, J. L. Vincent, and G. Ramsay; SCCM/ESICM/ACCP/ATS/SIS, "2001 SCCM/ESICM/ACCP/ATS/SIS International sepsis definitions conference," Crit. Care Med. **31**(4), 1250–1256 (2003).
3. M. Odeh, "Sepsis, septicaemia, sepsis syndrome, and septic shock: the correct definition and use," Postgrad. Med. J. **72**(844), 66 (1996).
4. M. A. Matthay, G. A. Zimmerman, C. Esmon, J. Bhattacharya, B. Coller, C. M. Doerschuk, J. Floros, M. A. Gimbrone, Jr., E. Hoffman, R. D. Hubmayr, M. Leppert, S. Matalon, R. Munford, P. Parsons, A. S. Slutsky, K. J. Tracey, P. Ward, D. B. Gail, and A. L. Harabin, "Future research directions in acute lung injury: summary of a National Heart, Lung, and Blood Institute working group," Am. J. Respir. Crit. Care Med. **167**(7), 1027–1035 (2003).
5. J. Villar, J. Blanco, H. Zhang, and A. S. Slutsky, "Ventilator-induced lung injury and sepsis: two sides of the same coin?" Minerva Anestesiol. **77**(6), 647–653 (2011).
6. D. Di Giantomasso, C. N. May, and R. Bellomo, "Vital organ blood flow during hyperdynamic sepsis," Chest **124**(3), 1053–1059 (2003).
7. S. C. P. L. Shiramizo, A. R. Marra, M. S. Durão, Â. T. Paes, M. B. Edmond, and O. F. Pavão dos Santos, "Decreasing mortality in severe sepsis and septic shock patients by implementing a sepsis bundle in a hospital setting," PLoS ONE **6**(11), e26790 (2011).

#201079 - $15.00 USD Received 20 Nov 2013; revised 9 Jan 2014; accepted 20 Jan 2014; published 5 Mar 2014

8. F. Stüber, "Effects of genomic polymorphisms on the course of sepsis: is there a concept for gene therapy?" J. Am. Soc. Nephrol. **12**(Suppl 17), S60–S64 (2001).
9. J.-H. Wu, C.-Y. Chen, P.-N. Tsao, W.-S. Hsieh, and H.-C. Chou, "Neonatal sepsis: a 6-year analysis in a neonatal care unit in Taiwan," Pediatr. Neonatol. **50**(3), 88–95 (2009).
10. R. Daniels, "Surviving the first hours in sepsis: getting the basics right (an intensivist's perspective)," J. Antimicrob. Chemother. **66**(Suppl 2), ii11–ii23 (2011).
11. J.-L. Vincent, Y. Sakr, C. L. Sprung, V. M. Ranieri, K. Reinhart, H. Gerlach, R. Moreno, J. Carlet, J.-R. Le Gall, and D. Payen; Sepsis Occurrence in Acutely Ill Patients Investigators, "Sepsis in European intensive care units: Results of the SOAP study," Crit. Care Med. **34**(2), 344–353 (2006).
12. K. Yano, P. C. Liaw, J. M. Mullington, S.-C. Shih, H. Okada, N. Bodyak, P. M. Kang, L. Toltl, B. Belikoff, J. Buras, B. T. Simms, J. P. Mizgerd, P. Carmeliet, S. A. Karumanchi, and W. C. Aird, "Vascular endothelial growth factor is an important determinant of sepsis morbidity and mortality," J. Exp. Med. **203**(6), 1447–1458 (2006).
13. D. C. Angus, W. T. Linde-Zwirble, J. Lidicker, G. Clermont, J. Carcillo, and M. R. Pinsky, "Epidemiology of severe sepsis in the United States: analysis of incidence, outcome, and associated costs of care," Crit. Care Med. **29**(7), 1303–1310 (2001).
14. L. Liu, H. L. Johnson, S. Cousens, J. Perin, S. Scott, J. E. Lawn, I. Rudan, H. Campbell, R. Cibulskis, M. Li, C. Mathers, and R. E. Black; Child Health Epidemiology Reference Group of WHO and UNICEF, "Global, regional, and national causes of child mortality: an updated systematic analysis for 2010 with time trends since 2000," Lancet **379**(9832), 2151–2161 (2012).
15. J. E. Lawn, S. Cousens, and J. Zupan; Lancet Neonatal Survival Steering Team, "4 million neonatal deaths: When? Where? Why?" Lancet **365**(9462), 891–900 (2005).
16. S. L. Zanotti-Cavazzoni and R. P. Dellinger, "Hemodynamic optimization of sepsis-induced tissue hypoperfusion," Crit. Care **10**(Suppl 3), S2 (2006).
17. T. Koch, S. Geiger, and M. J. R. Ragaller, "Monitoring of organ dysfunction in sepsis/systemic inflammatory response syndrome: Novel strategies," J. Am. Soc. Nephrol. **12**(Suppl 17), S53–S59 (2001).
18. M. D. Menger, B. Vollmar, and K. Messmer, "Sepsis and nutritional blood flow," in *Sepsis*, P. D. K. Reinhart, P. D. K. Eyrich, and P. D. C. Sprung, ed. (Springer Berlin Heidelberg, Berlin, 1994).
19. K. D. Fairchild and T. M. O'Shea, "Heart rate characteristics: Physiomarkers for detection of late-onset neonatal sepsis," Clin. Perinatol. **37**(3), 581–598 (2010).
20. E. Rivers, B. Nguyen, S. Havstad, J. Ressler, A. Muzzin, B. Knoblich, E. Peterson, and M. Tomlanovich; Early Goal-Directed Therapy Collaborative Group, "Early goal-directed therapy in the treatment of severe sepsis and septic shock," N. Engl. J. Med. **345**(19), 1368–1377 (2001).
21. A. Kumar, D. Roberts, K. E. Wood, B. Light, J. E. Parrillo, S. Sharma, R. Suppes, D. Feinstein, S. Zanotti, L. Taiberg, D. Gurka, A. Kumar, and M. Cheang, "Duration of hypotension before initiation of effective antimicrobial therapy is the critical determinant of survival in human septic shock," Crit. Care Med. **34**(6), 1589–1596 (2006).
22. T. J. Love, "Thermography as an indicator of blood perfusion," Ann. N. Y. Acad. Sci. **335**(1 Thermal Chara), 429–437 (1980).
23. E. F. J. Ring, H. McEvoy, A. Jung, J. Zuber, and G. Machin, "New standards for devices used for the measurement of human body temperature," J. Med. Eng. Technol. **34**(4), 249–253 (2010).
24. R. B. Knobel, B. D. Guenther, and H. E. Rice, "Thermoregulation and thermography in neonatal physiology and disease," Biol. Res. Nurs. **13**(3), 274–282 (2011).
25. L. B. Rowell, *Human Circulation: Regulation during Physical Stress* (Oxford University Press, 1986).
26. O. J. Garden, A. W. Bradbury, J. L. R. Forsythe, and R. W. Parks, *Principles and Practice of Surgery* (Elsevier Health Sciences, 2012).
27. A. K. Abbas, K. Heimann, K. Jergus, T. Orlikowsky, and S. Leonhardt, "Neonatal non-contact respiratory monitoring based on real-time infrared thermography," Biomed. Eng. Online **10**(1), 93 (2011).
28. M. Garbey, N. Sun, A. Merla, and I. Pavlidis, "Contact-free measurement of cardiac pulse based on the analysis of thermal imagery," IEEE Trans. Biomed. Eng. **54**(8), 1418–1426 (2007).
29. K. Heimann, K. Jergus, A. K. Abbas, N. Heussen, S. Leonhardt, and T. Orlikowsky, "Infrared thermography for detailed registration of thermoregulation in premature infants," J. Perinat. Med. **41**(5), 613–620 (2013).
30. G. F. Lewis, R. G. Gatto, and S. W. Porges, "A novel method for extracting respiration rate and relative tidal volume from infrared thermography," Psychophysiology **48**(7), 877–887 (2011).
31. N. Memarian, A. N. Venetsanopoulos, and T. Chau, "Infrared thermography as an access pathway for individuals with severe motor impairments," J. Neuroeng. Rehabil. **6**(1), 11 (2009).
32. A. Merla and G. L. Romani, "Functional infrared imaging in medicine: A quantitative diagnostic approach," in *Proceedings of IEEE Engineering in Medicine and Biology Society* (Institute of Electrical and Electronics Engineers, New York, 2006), pp. 224–227.
33. G. C. Wishart, M. Campisi, M. Boswell, D. Chapman, V. Shackleton, S. Iddles, A. Hallett, and P. D. Britton, "The accuracy of digital infrared imaging for breast cancer detection in women undergoing breast biopsy," Eur. J. Surg. Oncol. **36**(6), 535–540 (2010).
34. M. Czaplik, I. Biener, R. Dembinski, P. Pelosi, T. Soodt, W. Schroeder, S. Leonhardt, G. Marx, R. Rossaint, and J. Bickenbach, "Analysis of regional compliance in a porcine model of acute lung injury," Respir. Physiol. Neurobiol. **184**(1), 16–26 (2012).
35. N. Otsu, "A threshold selection method from gray-level histograms," IEEE Trans. Syst. Man Cybern. **9**(1), 62–66 (1979).

#201079 - $15.00 USD Received 20 Nov 2013; revised 9 Jan 2014; accepted 20 Jan 2014; published 5 Mar 2014

36. T. Berger, J. Green, T. Horeczko, Y. Hagar, N. Garg, A. Suarez, E. Panacek, and N. Shapiro, "Shock index and early recognition of sepsis in the emergency department: Pilot study," West J. Emerg Med **14**(2), 168–174 (2013).
37. Y. Yasaka, R. G. Khemani, and B. P. Markovitz, "Is shock index associated with outcome in children with sepsis/septic shock?*," Pediatr. Crit. Care Med. **14**(8), e372–e379 (2013).
38. M. Y. Rady, P. Nightingale, R. A. Little, and J. D. Edwards, "Shock index: a re-evaluation in acute circulatory failure," Resuscitation **23**(3), 227–234 (1992).
39. S. L. Weinberg and S. K. Abramowitz, *Statistics using SPSS: An integrative approach* (Cambridge University Press, 2008).
40. K. F. W. Messmer, "Traumatic shock in polytrauma: Circulatory parameters, biochemistry, and resuscitation," World J. Surg. **7**(1), 26–30 (1983).

1. Introduction

Acute circulatory disorders belong to the major causes of death. In critical care medicine, this complication often takes its course starting with *systemic inflammatory response syndrome* (SIRS) or *sepsis*.

Sepsis is a severe disease characterized by the presence of both *infection* and *SIRS*. It might develop into *severe sepsis* or *septic shock*. While the former corresponds to an aggravated sepsis by acute organ dysfunction, the latter corresponds to a severe sepsis plus hypotension, which is not reversed with fluid resuscitation [1–3]. Although there are several diseases leading to SIRS and sepsis, acute lung injury (ALI) and pulmonary infection are still considered the major causes of them [4]. Besides, several pathophysiological similarities and links have been stated by diverse studies [5].

Severe sepsis and septic shock are the main factors of morbidity and mortality in both, intensive care units (ICUs) [6–8], and neonatal intensive care units (NICUs) [9]. According to the literature, this pathology presents a wide range of incidence and, consecutively, a great impact concerning healthcare resources and expenditure [10,11]. In the United States, 751,000 cases of severe sepsis are considered to occur annually with a mortality that reaches 28.6% [11–13]. This astonishing number corresponds to a national estimation of the year 1995 presented by Angus and co-authors (2001) [13]. Moreover, a study carried out by Lawn and associates [14] indicated severe infections (including sepsis/pneumonia, tetanus, and diarrhea) as the second major cause of death in neonates (0-27 days). According to this publication, of 3.072 million deaths in 2010, approximately 27% were attributed to these complications, i.e. to severe infections [14,15].

Cavazzoni et al. [16] affirm that during sepsis, cardiovascular changes arise. This phenomenon may lead to tissue hypoperfusion, a determining factor in the development of multiple organ dysfunction [16–18]. Thus, to improve the outcome of the patients through appropriate clinical interventions (e.g. antibiotic therapy and organ support) an early diagnosis must be performed [1,19,20]. In an outstanding publication, Kumar et al. [21] evidenced an increase of 7.6% in mortality rate for every hour by which antimicrobials were tardily administered. However, early identification and application of appropriate therapy is a constant challenge for clinicians, since signs and symptoms of sepsis are nonspecific [21].

In 1980 Love [22] claimed that thermal emission of a living body is associated with its so called metabolic heat, which is, in turn, proportional to regional perfusion. Therefore, body temperature is a vital physiological parameter which supports defining health and disease, so that, knowledge of the skin's temperature progress and its distribution might be highly important in case of illness. This parameter can give information about the degree and severity of an attack as well as indicate the progress of a disease (e.g., relapses and ameliorations) and therapeutic efficiency [23,24].

Body temperature is extremely dependent on the heat-exchange processes between skin, inner tissues, and vasculature, as well as on air-tissue interface, metabolic activity and sympathetic and parasympathetic activity. For this reason, its distribution may provide evidence of the centralization's progress, which means restriction of blood flow to vital organs (e.g., the brain, heart, lung, kidneys, spleen, and liver) at the expense of peripheral organs (e.g. skin and gut) [25,26].

#201079 - $15.00 USD Received 20 Nov 2013; revised 9 Jan 2014; accepted 20 Jan 2014; published 5 Mar 2014

Medical infrared thermography is a remote, non-invasive and non-contact monitoring technique that permits to investigate the physiological functions associated with skin temperature control. Since skin temperature distribution depends on diverse physiologic processes (previously referred), infrared thermography (IRT) has become a promising imaging technology for medical applications [27–33]. Moreover, it is important to emphasize that IRT is a passive method, i.e. just records the radiation naturally emitted from the skin, and does not utilize any harmful radiation [27].

The current study investigates whether IRT is capable (a) of detecting acute impairments of body circulation and perfusion as well as (b) of monitoring the progress of temperature centralization in a porcine animal model of ALI. Therefore, the main goal of this paper is to analyze the capability of two indexes (standard deviation and $\Delta T/\Delta x$, a spatial temperature gradient) to quantify peripheral temperature gradients and, consecutively, peripheral perfusion.

2. Material and methods

2.1 Animal trial – experimental protocol

The current study corresponds to an amendment of the experimental protocol that was approved by the governmental institution "*Landesamt für Natur, Umwelt und Verbraucherschutz NRW*" (Germany; 84-02.04.2012.A173). It was performed according to the declaration of Helsinki and the guiding principles in the care and use of animals.

For these supplementary measurements, six of the study pigs, weighing 31.7-39.9 kg (approximately 12-14 weeks old) were randomly selected and numbered from 1 to 6. A veterinarian confirmed the absence of pre-existing diseases at the beginning of the study.

The animals were anesthetized, intubated and placed in supine position, as depicted in Fig. 1. To maintain the anesthesia, infusions of thiopental (7-12 mg kg^{-1} h^{-1}) and fentanyl (6-10 µg kg^{-1} h^{-1}) were continuously administered. Besides that, a 5 ml kg^{-1} h^{-1} Ringer solution for fluid replacement was continuously administrated and adapted to current needs of the animals. For volume balancing, a transurethral bladder catheter was inserted.

Approximately one hour after initiation of anesthesia and baseline measurements, experimental ALI was induced. This was performed by repeated surfactant washout [34]. Circa two hours after this step was completed, dependent on the number of repetitions needed to induce ALI, the first measurement under ALI, named ALI 1, took place. Controlled mechanical ventilation was set by using a variable PEEP, which was adjusted according physiological responses, and an inspiration:expiration ratio of 1:1. Subsequently, regular acquisition of vital data, blood gas analysis and further measurements were performed as well as infrared data recording.

At the end of the protocol, i.e. twenty-four hours after the measurement point ALI 1, the animals were euthanized by applying a deep analog sedation (Fig. 2).

#201079 - $15.00 USD Received 20 Nov 2013; revised 9 Jan 2014; accepted 20 Jan 2014; published 5 Mar 2014

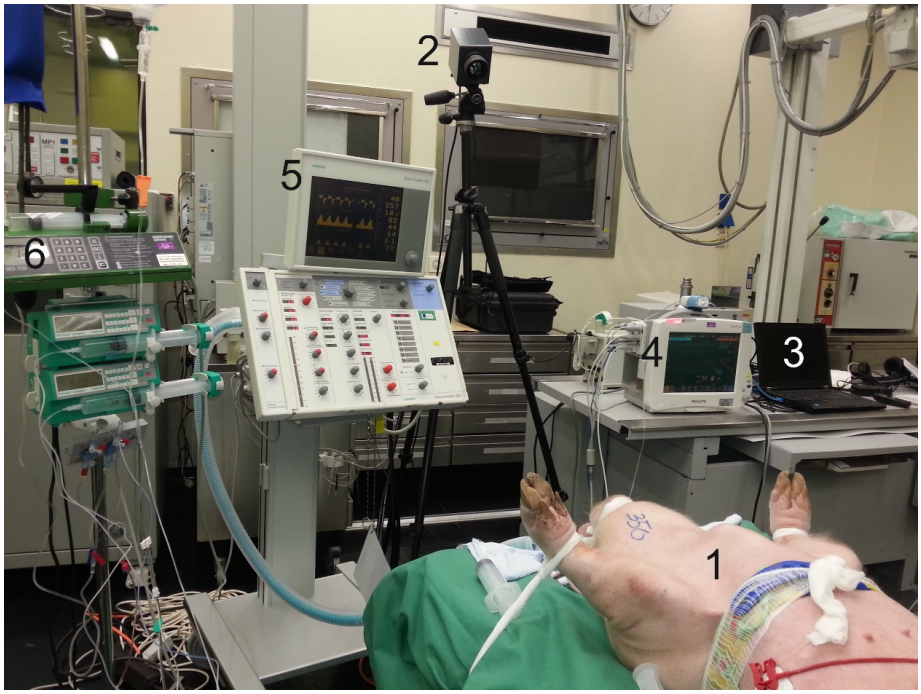

Fig. 1. Photography of the experimental setup (1: anesthetized animal; 2: infrared camera; 3: laptop; 4: patient monitoring system (Philips IntelliVue MP 70, Philips Medical Systems, Eindhoven, Netherlands); 5: Ventilator (Siemens 300A Servo Ventilator, Siemens Healthcare, Munich, Germany) and 6: Syringe pumps).

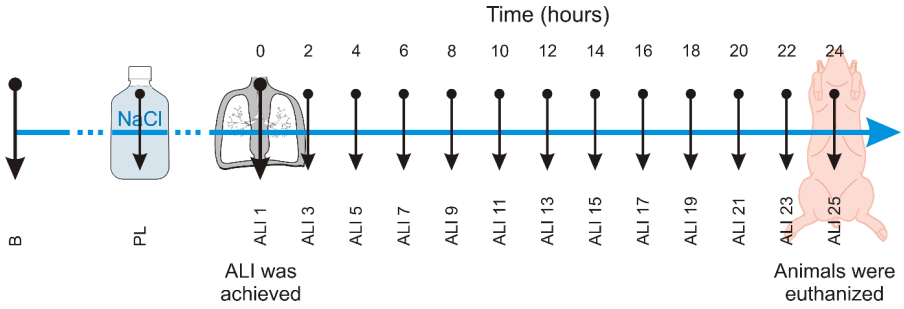

Fig. 2. Chronogram representing all the measurement time points (B: Baseline; PL: Post-lavage; ALI: acute lung injury).

2.2 Infrared data acquisition and experimental setup

Infrared (IR) thermograms were collected in this animal trial by using a long wave infrared (LWIR) camera, VarioCAM® hr head (InfraTec GmbH, Dresden, Germany), pre-calibrated, with a thermal sensitivity of 0.03 °C at 30 °C (Fig. 3). It detects IR wavelengths in the spectral range of 7.5-14 µm and presents a spatial resolution of 384 x 288 pixels. Additionally, the current device allows a capturing rate of 50 frames per second (fps) via FireWire (IEEE1394).

For image acquisition, the camera was sat atop a tripod and connected to a standard laptop computer via FireWire (IEEE1394) (Fig. 3). Subsequently, the tripod was placed approximately 1.5-2 m away from the examination table and its angle regulated (approximately 40°) (Fig. 1). Body parts such as head, superior limbs and trunk were predefined as a whole region of interest (ROI). Thus, the camera was positioned so that they

#201079 - $15.00 USD Received 20 Nov 2013; revised 9 Jan 2014; accepted 20 Jan 2014; published 5 Mar 2014

could be embraced in the thermograms. In addition to that, the position of the tripod and the angle of the camera were maintained constant, to avoid differences between thermograms.

In order to evaluate the evolution of skin temperature distribution, measurements with this IR camera were performed. They were carried out (1) at the beginning of the animal trial (baseline measurement - B), (2) after ALI was induced (post-lavage - PL), (3) at measuring point ALI 1, and subsequently, (4) at two-hourly intervals (ALI 3 to 25) (Fig. 2). For subsequent analysis of skin temperature distribution only one representative frame for each measurement time point was used.

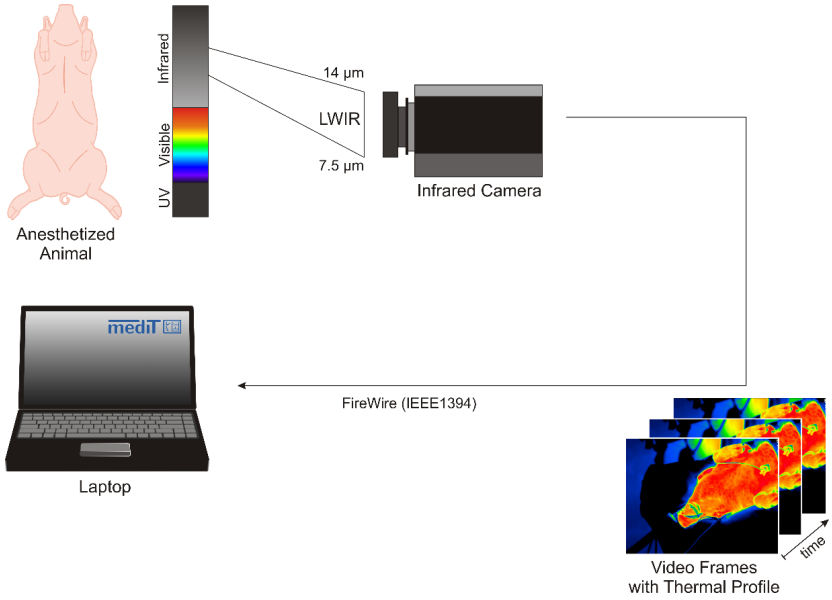

Fig. 3. Schematic of the experimental setup used in the animal trial.

2.3 Vital data acquisition

In addition to temperature monitoring, assessment of vital parameters such as heart rate (HR), blood pressure (systolic, mean and diastolic blood pressure), and saturation of peripheral oxygen (S_pO_2) was performed. For this purpose, a patient monitoring system (Philips IntelliVue MP 70, Philips Medical Systems, Eindhoven, Netherlands) was used (Fig. 1). Furthermore, blood samples were collected and arterial blood gas analysis (BGA) (ABL 510, Radiometer, Copenhagen, Denmark) carried out to determine the amount of oxygen and carbon dioxide dissolved in arterial blood (P_aO_2 and P_aCO_2) as well as the current pH.

2.4 Thermal images processing

Besides the anesthetized animals, appearance of other objects (e.g. monitoring devices, operating table, and blankets) in the thermograms was in some cases unavoidable. Therefore, image segmentation was necessary. For this reason, the method developed by Nobuyuki Otsu [35] called a *clustering-based method*, which permits to adaptively determine an optimal intensity threshold (in this case an optimal temperature threshold), was adopted [31]. It considers that an image is composed of two classes of pixels - *foreground* and *background*. Hence, using discriminant analysis, the algorithm estimates an optimal threshold value (T*) separating those classes by minimizing the *within-class variance* - σ^2_{wcv}, or equivalently, by maximizing the *between-class variance* - σ^2_{bcv}:

$$T^* = \arg\max_{0 \le T \le L} \left\{ \sigma^2_{bcv}(T) \right\}. \quad (1)$$

#201079 - $15.00 USD Received 20 Nov 2013; revised 9 Jan 2014; accepted 20 Jan 2014; published 5 Mar 2014

The *between-class variance* is given by

$$\sigma_{bcv}^2(T) = \sigma^2(T) - \sigma_{wcv}^2(T), \tag{2}$$

where σ^2 represents the total variance and T a threshold value. The *within-class variance* corresponds, on the other hand, to the weighted sum of the variances of each cluster [σ_B^2: variance of the pixels in the background; σ_F^2 : variance of the pixels in the foreground] as defined by:

$$\sigma_{wcv}^2(T) = \omega_B(T)\sigma_B^2(T) + \omega_F(T)\sigma_F^2(T), \tag{3}$$

where the probabilities of the two classes - background and foreground - are

$$\omega_B(T) = \sum_{i=0}^{T-1} p(i), \tag{4}$$

$$\omega_F(T) = \sum_{i=T}^{L-1} p(i). \tag{5}$$

It is valuable to note, that in our notation the temperature ranges from 0 to L-1, where L represents a distinct temperature. The probability of occurrence of temperature i is formulated, in turn, as

$$p(i) = n(i) / N. \tag{6}$$

In this equation, n(i) corresponds to the number of pixels with temperature i and N represents the total number of pixels in a certain image.

The *between-class variance* equation [Eq. (1)] previously introduced can be further computed as

$$\sigma_{bcv}^2(T) = \omega_B(T)\left[\mu_B(T) - \mu\right]^2 + \omega_F(T)\left[\mu_F(T) - \mu\right]^2, \tag{7}$$

where the mean temperature values of the entire image [Eq. (8)] as well as of both classes [(Eq. (9) and Eq. (10)] are defined as:

$$\mu(T) = \sum_{i=0}^{L-1} ip(i), \tag{8}$$

$$\mu_B(T) = \sum_{i=0}^{T-1} ip(i)/\omega_B(T), \tag{9}$$

$$\mu_F(T) = \sum_{i=T}^{L-1} ip(i)/\omega_F(T). \tag{10}$$

In order to fill the holes (defined as set of background pixels that does not contact with the background) in the binary image, preprocessing was required. After segmentation, several small regions, which did not correspond to foreground, but to the background, were not efficiently extracted, since their temperature is higher than the adaptively estimated threshold. Therefore, it was considered that only the biggest region corresponds to the ROI. The preprocessing algorithms previously described were implemented in MATLAB (MATLAB 2013a, The MathWorks Inc., Natick, MA).

2.5 Statistical analysis

In order to evaluate the skin temperature distribution, the index $\Delta T/\Delta x$, which can be considered as measure of the spatial temperature profile/gradient, was examined. It corresponds to the spatial change in temperature ΔT with distance Δx between the body center and the most peripheral collateral point visible in the thermogram. Therefore, just one hemisphere was considered. As the central reference point, the hottest point next to the coolish sternal region was chosen with the shortest distance to the peripheral point (paw) (Fig.

#201079 - $15.00 USD Received 20 Nov 2013; revised 9 Jan 2014; accepted 20 Jan 2014; published 5 Mar 2014

4). It should be noted that similar approaches have already been integrated in image processing software. The temperature gradient as well as the standard deviation (SD) of the skin temperature distribution were correlated with mean arterial pressure (MAP), shock index (SI), P_aO_2 and P_aO_2/F_iO_2 as indications for circulatory impairments and oxygenation, respectively. SI, defined as the ratio of heart rate to systolic blood pressure, is a marker of shock. According to some research groups, this parameter is an effective marker for the initial assessment of sepsis [36,37] and presents a great physiologic significance in acute circulatory failure [38]. The parameter P_aO_2/F_iO_2, also denominated PF ratio, corresponds to the ratio of arterial oxygen concentration to the fraction of inspired oxygen. In Critical Care medicine and Anesthesiology, it permits to describe the severity of pulmonary dysfunction.

Statistical analysis was performed in SPSS version 19.0 (SPSS Inc., IBM Business Analytics Software, Armonk, New York, USA). To calculate correlation between variables, Pearson's method was applied. Moreover, normal distribution of data was determined by carrying out the Kolmogorov-Smirnov test. Since normal distribution was corroborated, one-way analysis of variance (ANOVA) was used for the assessment of statistical differences between time points. Additionally, histogram analysis was also effectuated. To describe shape characteristics of a distribution, skewness and kurtosis were studied. A p-value of <0.05 was considered as level of significance. Outliers are marked in boxplots but not removed from statistical analysis.

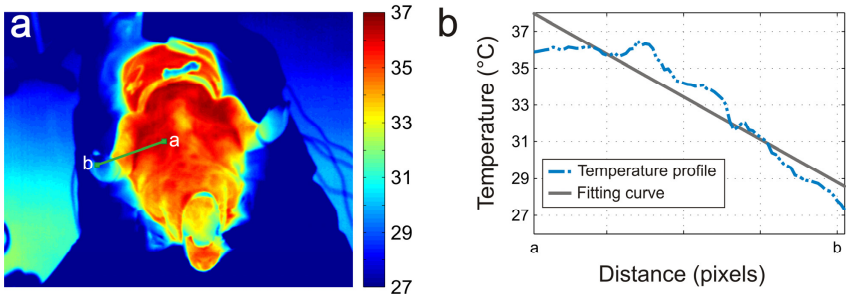

Fig. 4. (a) Thermogram with temperature profile. (b) Graphic representation of the temperature profile (Dash-dot line - blue) as well as of the fitting curve (solid line - gray). $\Delta T/\Delta x$ correspond to the slope of the fitting curve ($\Delta T/\Delta x = 0.1160$).

3. Results

In the current study, six young female pigs weighing 35.18 ± 3.63 kg (mean ± SD), were studied. Owing to consequences of acute respiratory distress syndrome (ARDS) (severe circulatory instability with the need of high amounts of catecholamines and severe hypoxia), three animals died before the end of the animal trial but all hitherto data were analyzed (one pig died at ALI 9 and the remaining two at ALI 17). All results presented below are expressed as mean ± SD.

As previously referred, image pre-processing was required to define the ROI (head, superior limbs and trunk). In order to show the performance of the pre-processing algorithm as well as to illustrate the development of the skin temperature distribution, six thermograms were selected. They correspond to the same animal and represent six different time points (baseline, ALI 1, ALI 7, ALI 13, ALI 19, and ALI 25). Figure 5 depicts the original thermograms as well as the thermograms after pre-processing. In addition, the same figure includes the histograms corresponding to the pre-processed thermal images, which contain the ROI (head, superior limbs and trunk). Major characteristics of the acquired thermograms are: occurrence of spotty markings after ALI induction, varying mean temperature and distribution as well as increasing temperature gradients from the periphery to the center. In order to study the distribution shape of the histograms, both kurtosis and skewness were investigated (Fig. 6).

#201079 - $15.00 USD Received 20 Nov 2013; revised 9 Jan 2014; accepted 20 Jan 2014; published 5 Mar 2014

Figure 7 represents, in turn, the relationship between SI, MAP, SD and ΔT/Δx over the fifteen measurement time points. This graphic illustration exhibits a similar tendency between SD and ΔT/Δx. Although it is inversely proportional, MAP presents an analogous behavior to the previous parameters (SD and ΔT/Δx). Regarding SI, it is important to emphasize that there is no significant difference between groups, i.e. between each measurement time point. Nevertheless, the course of SI is similar to the one of SD and ΔT/Δx, which is particularly noticeable between ALI 11 and ALI 19, so that corresponding correlations are strong (Fig. 7).

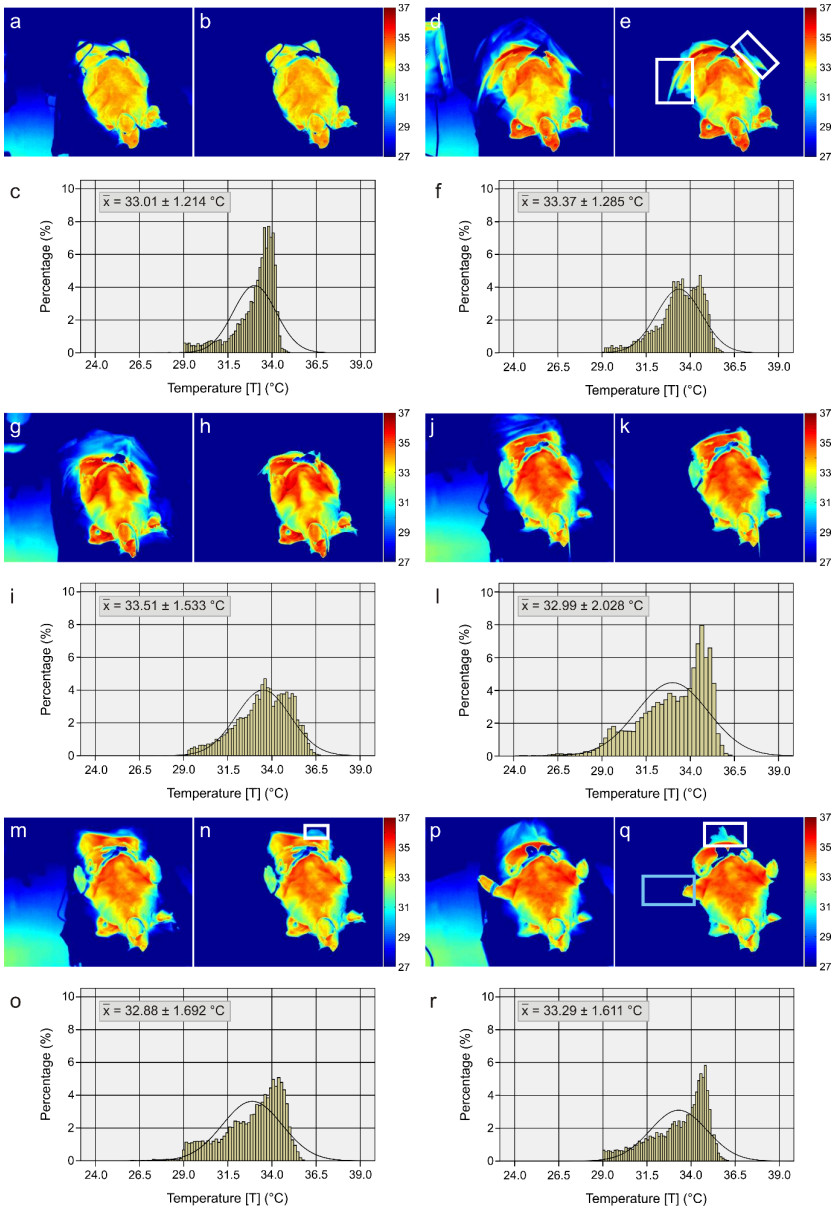

Fig. 5. Original thermograms at six differing points of time [(a) Baseline, (d) ALI 1, (g) ALI 7, (j) ALI 13, (m) ALI 19, (p) ALI 25]. Thermograms representing ROIs after pre-processing [(b) Baseline, (e) ALI 1, (h) ALI 7, (k) ALI 13, (n) ALI 19, (q) ALI 25]. Histograms representing the relative skin temperature distribution of the ROIs (head, superior limbs and trunk) [(c) Baseline, (f) ALI 1, (i) ALI 7, (l) ALI 13, (o) ALI 19, (r) ALI 25]. Regarding the white frames (e, n, q), they identify regions that were not properly extracted. The blue frame (q) defines a region that was wrongly considered as background.

#201079 - $15.00 USD Received 20 Nov 2013; revised 9 Jan 2014; accepted 20 Jan 2014; published 5 Mar 2014

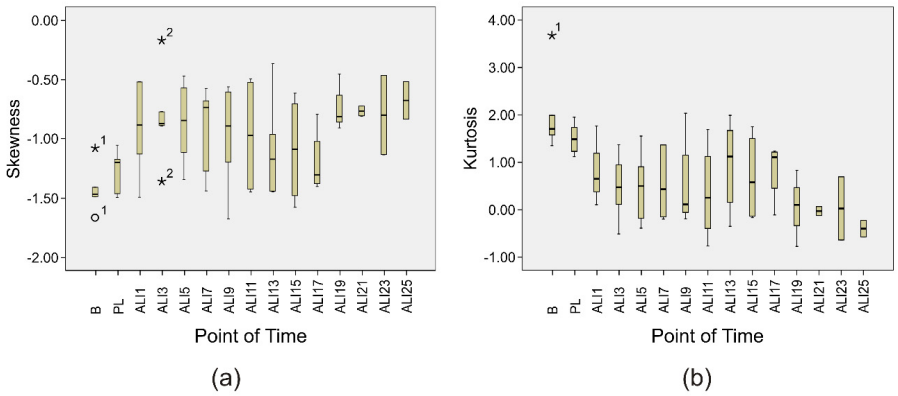

Fig. 6. Boxplots describing the course of (a) Skewness and (b) Kurtosis over the measurement points. The outliers are identified with the number of the corresponding animal ("o" and "*" stand for mild (between 1.5 and 3x interquartile range) and extreme (>3x interquartile range) outliers, respectively).

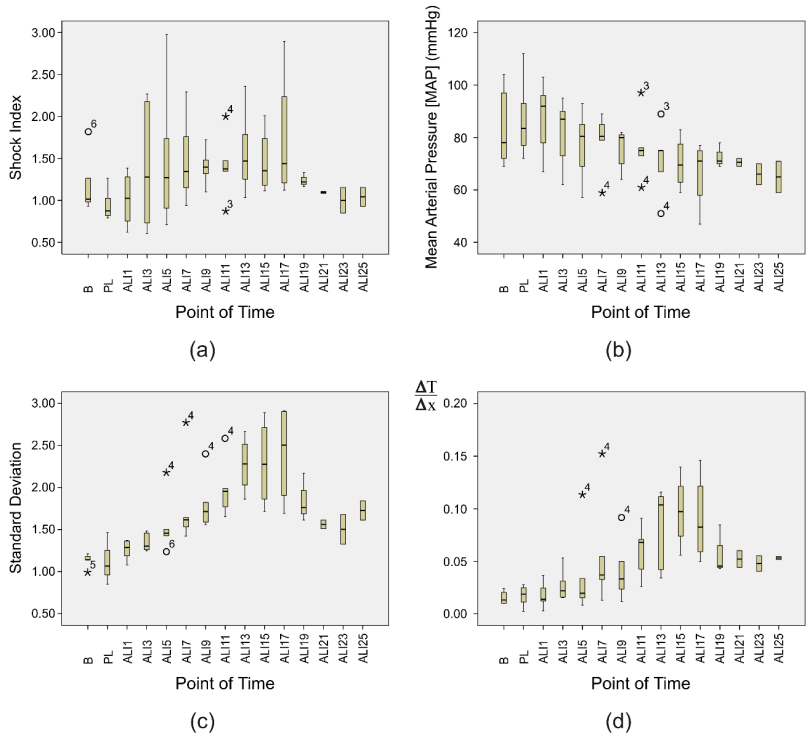

Fig. 7. Boxplots describing the course of (a) Shock index (SI), (b) mean arterial pressure (MAP), (c) standard deviation (SD) and (d) $\Delta T/\Delta x$ over the fifteen measurement points [B (baseline), PL (post-lavage), ALI 1, ALI 3, ALI 5, ALI 7, ALI 9, ALI 11, ALI 13, ALI 15, ALI 17, ALI 19, ALI 21, ALI 23 and ALI 25]. Difference between groups are significant for $\Delta T/\Delta x$ ($p<0.0005$) and SD ($p<0.0005$). The outliers are identified with the number of the corresponding animal ("o" and "*" stand for mild (between 1.5 and 3x interquartile range) and extreme (>3x interquartile range) outliers, respectively).

With the purpose of illustrating the progress of pulmonary dysfunction and oxygen levels in blood, two further variables, P_aO_2 and PF ratio, were analyzed (Fig. 8).

#201079 - $15.00 USD Received 20 Nov 2013; revised 9 Jan 2014; accepted 20 Jan 2014; published 5 Mar 2014

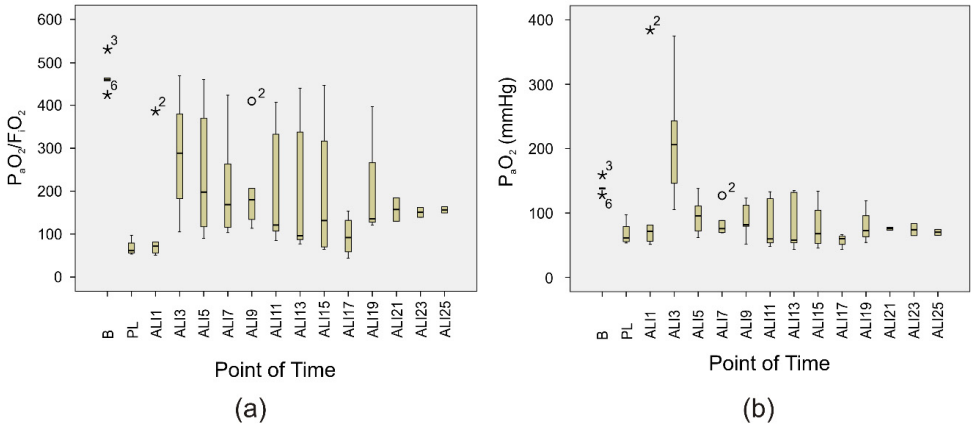

Fig. 8. Boxplots describing the course of (a) PF ratio and (b) P_aO_2 over the fifteen measurement points. Difference between groups are significant for P_aO_2 (p=0.006) and PF ratio (p=0.002). The outliers are identified with the number of the corresponding animal ("o" and "*" stand for mild (between 1.5 and 3x interquartile range) and extreme (>3x interquartile range) outliers, respectively).

Regarding statistical analysis, the one-way ANOVA indicated significant differences for four parameters, SD [$F(14,53) = 7.385$, $p<0.0005$], $\Delta T/\Delta x$ [$F(14,53) = 3.687$, $p<0.0005$], P_aO_2 [$F(14,53) = 2.622$, $p = 0.006$], PF ratio [$F(14,53) = 2.925$, $p = 0.002$]. In contrast, there were no statistically significant differences for MAP [$F(14,53) = 1.560$, $p = 0.122$] and SI [$F(14,53) = 1.031$, $p = 0.438$].

A Pearson product-moment correlation was used to determine the relationship between variables, which were in each case normally distributed. Correlation coefficients and levels of significance are described in Table 1. Among others, this method demonstrated strong significant correlations between the two proposed parameters (SD and $\Delta T/\Delta x$) and SI and MAP.

Table 1. Pearson product moment correlations between SD, $\Delta T/\Delta x$, SI and SI, MAP, P_aO_2 and PF ratio

		Standard Deviation	$\Delta T/\Delta x$	Shock Index
SI	Pearson Correlation	0.593§,*	0.561§,*	-
	p-value	<0.0005	<0.0005	-
MAP	Pearson Correlation	–0.587§,*	–0.534§,*	–0.519§,*
	p-value	<0.0005	<0.0005	<0.0005
P_aO_2	Pearson Correlation	–0.344§,**	–0.334§,**	–0.326§,**
	p-value	0.004	0.005	0. 007
PF ratio	Pearson Correlation	–0.315§,**	–0.319§,**	–0.326§,**
	p-value	0.009	0.008	0. 007

§ Correlation is significant at the 0.01 level (two-tailed).
* Strong correlation [0.40 < |r| < 0.70] - According to Weinberg *et al.* [39].
** Moderate Correlation [0.30 < |r| < 0.39] - According to Weinberg *et al.* [39].

4. Discussion

The present study aims to evaluate whether IRT is capable of remotely monitoring disturbances in circulation and perfusion. For this purpose, six pigs with experimentally induced ALI were analyzed. As referred, ALI is a very common disease in critical care and is one of the leading causes of SIRS and sepsis.

Image processing of the thermograms was imperative in order to remove the background. The performance and quality of background extraction was assessed visually. Therefore, according to our pre-established criteria, a satisfying background extraction must accurately

#201079 - $15.00 USD Received 20 Nov 2013; revised 9 Jan 2014; accepted 20 Jan 2014; published 5 Mar 2014

define the desired ROI, i.e. the upper body of the animals (head, superior limbs and trunk). The adaptive threshold method developed by Otsu [35] has demonstrated a good performance as illustrated by the examples in Fig. 5. Despite of good performance, some small regions were not properly extracted. This may be due to contrast/temperature similarity between the object (anesthetized animal) and the background. Figure 5 depicts a few examples marked with white frames. As referred, after segmentation, several regions were erroneously considered as foreground. Hence, it was assumed that just the biggest region corresponds to the ROI. Due to this assumption the region corresponding to the animal's paw, marked with a blue frame in Fig. 5(q), was removed. Despite the satisfying results achieved, in subsequent studies performance of several segmentation algorithms should be examined due to their high dependency on the clinical application.

The same figure (Fig. 5) displays the development of the skin temperature distribution. Firstly, at the baseline, the body temperature is uniformly distributed. However, thereafter it tends to centralize (the temperature profile is composed by a wide range of temperatures, decreasing from the center to the periphery) due to peripheral hypoperfusion, which results from the further progress of the disease's severity. The six histograms together with the SDs and $\Delta T/\Delta x$ (Fig. 7(c) and 7(d)) allow to sustain the previous affirmations.

Moreover, differences of shape of the probability distributions between baseline and ALI are evidenced. At baseline, the histograms tend to present both a higher negative asymmetry (left-skewed distribution - extreme scores are on the higher end of the histogram) and a higher kurtosis distribution (sharper and longer peak). A sharper and longer peak means that the distribution is more clustered around the mean, thus, it will have a relatively smaller SD. In other words, the percentage of pixels around the mean temperature is higher, which leads to a more homogeneously distributed body temperature. On the other hand, during ALI the histograms present smaller negative asymmetries (the histograms tend to become more symmetrical) as well as lower kurtosis distributions (Fig. 5 and Fig. 6). A lower peak means that the distribution is less clustered around the mean, which signifies higher standard deviations and, consecutively, a heterogeneously distributed body temperature (e.g. due to temperature centralization).

As previously highlighted, SI, which is a good measure of hemodynamic in-/stability, presents a high significance in acute circulatory failure. Due to its clinical relevancy, possible correlations between SI and SD as well as SI and $\Delta T/\Delta x$ were investigated. As alluded, SD and $\Delta T/\Delta x$ represent the skin temperature distribution and gradient, respectively. The Pearson product-moment correlation have demonstrated a strong correlation between SD and SI as well as between $\Delta T/\Delta x$ and SI. Furthermore, the same method evidenced a strong negative correlation between both parameters, SD, $\Delta T/\Delta x$, and MAP. As widely known, sepsis and shock are characterized by an impaired blood flow to body tissues (hypoperfusion), which leads to temperature centralization [40], and commonly include hypotension [16]. Figure 7 demonstrates that the progress of the disease severity is accompanied by an increase in SD, $\Delta T/\Delta x$ and SI and a decrease in MAP.

In addition, this statistical method pointed out a moderate negative correlation between SD, $\Delta T/\Delta x$, SI and both P_aO_2 and PF. Besides hypoperfusion, circulatory disorders contribute also for tissue hypoxia (insufficient levels of oxygen in blood or tissue; decreased P_aO_2), since there is an inability to meet the oxygen demands of the tissues. A decrease of the PF ratio is also expected owing to an increase of the severity of the pulmonary dysfunction (Fig. 8). In Fig. 8 an increase of PF ratio after ALI 17 is observed. This indicates an improvement on gas exchange mechanisms of the lung. As expected, it is accompanied with decreases in SI, SD and $\Delta T/\Delta x$.

Unexpectedly, one of the animals (animal number 4) suffered from an arterial peripheral thrombosis at t = ALI 3. This phenomenon has led to a worsening of its clinical situation. Between ALI 3 and ALI 11 vital parameters such as HR, MAP, P_aO_2 and PF ratio deviated from the other animals. Even the measures of the new parameters, SD and $\Delta T/\Delta x$, turned out to be outliers (Fig. 7).

#201079 - $15.00 USD Received 20 Nov 2013; revised 9 Jan 2014; accepted 20 Jan 2014; published 5 Mar 2014

According to the one-way ANOVA, there was statistically significant difference between measurement time points for SD, $\Delta T/\Delta x$, P_aO_2 and PF ratio. Regarding SI and MAP, no significant differences were denoted. The previous factors support the hypothesis that SD and $\Delta T/\Delta x$ might be capable of better representing the course of the disease's severity (Fig. 7).

In the present study, the parameters SD and $\Delta T/\Delta x$ were compared with the wide-known SI. Whereas SI, SI x age, systolic blood pressure and heart rate are relatively easy to assess and in particular determinable in our study, other measures need more invasive equipping such as central venous catheter, arterial catheter or even a pulmonary artery catheter. Hence, more sophisticated parameters like stroke volume variation, intrathoracic blood volume index or cardiac index are not available in our trial just as in most patients in intensive care. Besides, even invasively derived parameters such as mentioned before, do not carry a guarantee to adequately monitor course of severity of circulation disorders. The appropriateness is rather dependent on the root case for the circulatory disorder, e.g. hemorrhagic shock, cardiogenic shock, toxic shock or even sepsis.

Although the encouraging results, the study has a few limitations that need to be addressed. First, no control group was considered. Even though, a uniform temperature distribution with moderate variance would be expected throughout the animal trial since an adapted and balanced volume restitution was performed. Nevertheless, for further studies a control group should be considered. Second, no comparative method or technique was used to validate our results, since there is no gold standard available measuring similar properties. Third, it must be taken into account that there are large inter-individual varieties concerning the course of the disease. Since this a common problem in biomedical studies, the only way to overcome this challenge is to examine larger study populations. Fourth, regarding body surface temperature measurements, there are certainly differences between pigs and human patients (e.g. due to skin thickness and body fat). Unfortunately, no studies analyzing temperature distribution in pigs could be found in literature. Fifth, for IRT based circulation monitoring exposure of a large portion of the body is required. But, on the one hand, for diverse clinical applications such as examining regional perfusion it is not necessary to include the whole body but only some body parts. On the other hand, for other clinical applications requiring whole body examination, time limited uncovering of the patient (e.g. for 5 minutes) would also be practicable.

Another point to be addressed is the geometric arrangement of the IR camera. Ideally, it should be perpendicular to the body plane - ceiling-mounted. Since this project was a pilot study and several medical needs must to be considered [(1) the equipment must not prevent the anesthetist to perform its countless tasks according to the study protocol; (2) the need for several medical devices and equipment], a compromise had to be found for the location of this setup.

5. Conclusions

The current study demonstrated the capability of infrared thermography for monitoring circulation and perfusion in a porcine animal model. By developing adequate indexes, the course and severity of disease could be quantified. As expected, experimental ALI induced increases in both $\Delta T/\Delta x$ and SD, which is caused by temperature centralization and a risen heterogeneity in body temperature distribution In addition, significant correlations were shown between the latter indexes and the clinically established shock index.

Based on this pilot study, further trials should be carried out in order to prove these results and to establish new clinical fields of application, such as early detection and monitoring of sepsis and the efficacy of therapeutic procedures. The aim should be to receive medical implications within a time frame of several minutes to generate highest possible clinical benefits. In our opinion this is a challenging but realistic goal requiring both, modified technical and organizational concepts. After proving possible applications for IRT, the next step should be integration of this technique into clinical algorithms. After all, novel techniques for the assessment of regional perfusion, micro- and macrocirculatory

#201079 - $15.00 USD Received 20 Nov 2013; revised 9 Jan 2014; accepted 20 Jan 2014; published 5 Mar 2014

hemodynamics, such as infrared thermography, might be promising alternatives to enhance and optimize diagnostics and treatments in critical care medicine.

Acknowledgments

C. B. Pereira wishes to acknowledge FCT (Foundation for Science and Technology in Portugal) for her PhD grant SFRH / BD / 84357 / 2012.

#201079 - $15.00 USD Received 20 Nov 2013; revised 9 Jan 2014; accepted 20 Jan 2014; published 5 Mar 2014